

Electrocatalytic O₂ Reduction by an Organometallic Pd(III) Complex via a Binuclear Pd(III) Intermediate

Soumalya Sinha and Liviu M. Mirica*



Cite This: *ACS Catal.* 2021, 11, 5202–5211



Read Online

ACCESS |



Metrics & More



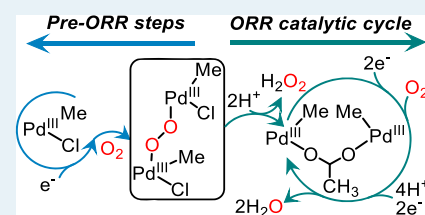
Article Recommendations



Supporting Information

ABSTRACT: The development of electrocatalysts for the selective O₂-to-H₂O conversion, the O₂ reduction reaction (ORR), is of great interest for improving the performance of fuel cells. In this context, molecular catalysts that are known to mediate the 4H⁺/4e⁻ reduction of O₂ to H₂O tend to be marred by limited stability and selectivity in controlling the multiproton and multielectron transfer steps. Thus, evaluation of transition metal complexes, including organometallic species, for ORR reactivity could uncover molecular catalysts with improved properties. We have previously reported the synthesis and characterization of various organometallic Pd^{III} complexes stabilized by the tetradentate ligand *N,N'*-di-*tert*-butyl-2,11-diaza[3.3](2,6)pyridinophane (^tBuN4). These complexes were shown to react with O₂ and undergo oxidatively induced C–C and C–heteroatom bond formation reactions in the presence of O₂. These O₂-induced oxidative transformations prompted us to evaluate the ORR reactivity of such organometallic Pd complexes, which to the best of our knowledge has never been studied before for any molecular Pd catalyst. Herein, we report the ORR reactivity of the [^t(BuN4)Pd^{III}MeCl]⁺ complex under both homogeneous and heterogeneous conditions in a nonaqueous and acidic aqueous electrolyte, respectively. Cyclic voltammetry and hydrodynamic electrochemical studies for [^t(BuN4)Pd^{III}MeCl]⁺ revealed that the electrocatalytic reduction of O₂ to H₂O proceeds with Faradaic efficiencies (FEs) of 50–70% in the presence of acetic acid (AcOH) in MeCN. The selectivity toward H₂O production further improved the FE to 80–90% in an acidic aqueous medium (pH 0), upon immobilization of the molecular catalyst onto edge plane graphite (EPG) electrodes. Analysis of electrochemical data suggests the formation of a binuclear Pd^{III} intermediate in solution, likely a Pd^{III}-peroxo-Pd^{III} species, which dictates the thermochemistry of the ORR process for [^t(BuN4)Pd^{III}MeCl]⁺ in MeCN, thus being a rare example of a bimolecular ORR process. The maximum second-order turnover frequency $\text{TOF}_{\text{max}}^2 = 2.76 \times 10^8 \text{ M}^{-1} \text{ s}^{-1}$ was determined for 0.32 mM of [^t(BuN4)Pd^{III}MeCl]⁺ in the presence of 1 M AcOH in O₂-saturated MeCN with an overpotential of 0.32 V. By comparison, a comparatively lower $\text{TOF}_{\text{max}}^2 = 1.25 \times 10^5 \text{ M}^{-1} \text{ s}^{-1}$ at a higher overpotential of 0.8 V was observed for [^t(BuN4)Pd^{III}MeCl]PF₆ adsorbed onto EPG electrodes in O₂-saturated 1 M H₂SO₄ aqueous solution. Overall, reported herein is a detailed ORR reactivity study using a Pd^{III} organometallic complex to benchmark its selectivity and energetics toward O₂ reduction in MeCN and acidic aqueous solutions.

KEYWORDS: organometallic Pd(III) complex, O₂ reduction reaction (ORR), homogeneous electrocatalysis, heterogeneous electrocatalysis, second-order ORR kinetics, second-order foot-of-the-wave analysis



INTRODUCTION

Proton exchange membrane fuel cells (PEMFCs) that can store and convert chemical energy into electricity are practical and promising devices that can provide an alternative to the use of fossil fuels.^{1,2} A simple model of a PEMFC can be described as a two-compartment cell, with the cathodic and anodic chambers separated by a polymer electrolyte or PEM. The anodic compartment splits H₂ molecules into 2H⁺ and 2e⁻, the protons being supplied to the cathodic compartment through the PEM, whereas the e⁻ transfer occurs through the external circuit to balance the voltage difference. The cathodic compartment performs the O₂ reduction reaction (ORR) by utilizing the provided protons and electrons to produce H₂O.³ Pt-based systems at both the anode and the cathode have been the most employed electrocatalysts in PEMFCs.^{1,4} In addition, although the development of earth-abundant materials for water splitting or H₂ oxidation has made significant progress,

finding robust and cost-effective materials as cathode catalysts for ORR is still an ongoing challenge.^{5,6}

Pd could be a choice to replace Pt because of its similarity in the crystal structure (face-centered cubic) and d-electronic configuration.⁷ In this regard, fuel cell relevant reactions such as electrochemical H₂ evolution or oxidation have shown progress by using Pd-based or carbon-supported Pd catalysts.^{8–10} Although pure metallic Pd is positioned very near to Pt in the volcano plot of ORR activity, as proposed by Nørskov and co-workers,¹¹ its use for electrochemical ORR is

Received: December 31, 2020

Revised: February 27, 2021

Published: April 15, 2021



limited as an additive for the reduction of Pt loading,^{12–14} while its reactivity is marred by the poor stability in acidic medium.^{15–17} In this regard, to the best of our knowledge, there is no Pd molecular system that has been reported to date as a catalyst for the electrochemical ORR reaction.¹⁸

Understanding homogeneous electrocatalysis has become important to benchmark the activity of molecular catalysts toward ORR. In this context, metalloporphyrins and metallophthalocyanines bearing first-row transition metals (e.g., Mn, Fe, and Co) have gained increased attention for electrocatalytic ORR.¹⁸ For example, Mn^{II} tetraphenylporphyrin and hangman porphyrin xanthene (Mn(HPX-CO₂H)), reported by Nocera et al., reduce O₂ with high selectivity, ≥75% toward H₂O in MeCN in the presence of acetic acid (AcOH) or its derivatives.¹⁹ Additional examples were provided by Mayer and co-workers for the homogeneous electrochemical ORR using different metalloporphyrin derivatives.^{18,20,21} Nevertheless, recent efforts made to incorporate such metalloporphyrins into pyrolytic graphite electrodes also provide heterogeneous ORR platforms with high selectivity toward H₂O production in an acidic aqueous medium that could have more impact on designing practical energy devices.^{22–24} However, the synthesis of porphyrins or its derivatives is often limited by low yields, which limits their potential industry-scale applications.

Thus, evaluation of new transition metal complexes, including organometallic species, for ORR reactivity could uncover new molecular catalysts with improved properties. We have previously reported the synthesis and characterization of various organometallic Pd^{III} complexes stabilized by the tetradentate ligand *N,N'*-di-*tert*-butyl-2,11-diaza[3.3](2,6)-pyridinophane (^tBuN4) and related analogues.^{25–28} These complexes were shown to react with O₂ and undergo oxidatively induced C–C and C–heteroatom bond formation reactions in the presence of O₂. These O₂-induced oxidative transformations prompted us to evaluate the ORR reactivity of such organometallic complexes, which to the best of our knowledge has never been done before for any molecular Pd catalyst. Herein, we report the ORR reactivity of the [(^tBuN4)Pd^{III}MeCl]PF₆ complex, **1•PF₆** (Figure 1), both

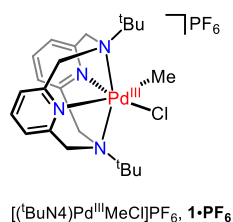


Figure 1. Organometallic Pd^{III} complex employed herein in the ORR studies.

under homogeneous and heterogeneous conditions in a nonaqueous and acidic aqueous electrolyte, respectively. First, we benchmarked the electrocatalytic activity toward ORR using **1•PF₆** in MeCN in the presence of AcOH, and then the same catalyst was immobilized onto an edge plane graphite (EPG) electrode to compare its performance in O₂-saturated 1 M H₂SO₄ aqueous solution at pH 0. Cyclic voltammetry and rotating-ring disk electrode voltammetry studies carried out for **1•PF₆** reveal high peak current density, 12 mA/cm² in O₂-saturated MeCN with 1 M of added AcOH and up to 70% selectivity for H₂O formation. Additionally, interpretation of the electrochemical data and “foot-of-the-

wave” analysis (FOWA) suggests that the reaction mechanism for O₂ reduction involves a binuclear Pd^{III} intermediate, likely a Pd^{III}-peroxo-Pd^{III} species. Second-order ORR rate constants (*k*_{ap}) of ~2.76 × 10⁵ M⁻¹ s⁻¹ at different catalyst concentrations were also extracted using FOWA.

By comparison, electrochemical data obtained for **1•PF₆** adsorbed onto EPG electrodes exhibited comparatively lower catalytic current densities, 0.5 mA/cm², but high selectivity (≥80%) toward H₂O formation in O₂-saturated 1 M aqueous H₂SO₄. At these conditions, Koutecký–Levich (K–L) plots were also constructed, and the number of electrons associated with the heterogeneous ORR catalysis is estimated to be between 3.74 and 4.03 from the slope of the linearly fitted K–L plots within the applied potential of 0.2 V and 0.1 V vs normal hydrogen electrode (NHE). Additionally, the intercepts of the linearly fitted K–L plots provided the overall second-order reaction rate constant as 1.25 × 10⁵ M⁻¹ s⁻¹ under these heterogeneous conditions. Overall, herein we report the ORR reactivity of an organometallic Pd^{III} complex and show that this species is an efficient and stable ORR electrocatalyst under both homogeneous and heterogeneous conditions in a nonaqueous and acidic aqueous electrolyte, respectively.

EXPERIMENTAL DETAILS

Reagents and Materials. All chemicals were commercially available from Aldrich, Fisher, or Strem Chemicals and were used as received without further purification. Solvents were purified prior to use by passing them through a column of activated alumina using an MBraun solvent purification system.

Synthesis and Characterization. Synthesis and detailed characterization of [(^tBuN4)Pd^{III}MeCl]PF₆, **1•PF₆**, were reported previously.²⁵

Electrochemical Studies. All electrochemical experiments were carried out using BASi Epsilon and CH Instruments potentiostats. Rotating ring-disk electrochemistry (RRDE) used glassy carbon (GC) as the disk and Pt-wire as the ring electrode, and all RRDE experiments were performed using the Pine Modulated Speed Rotator. All cyclic voltammograms (CVs) and RRDE data are plotted according to the “US convention”,²⁹ where the positive and negative currents are for the reduction and oxidation processes, respectively. All CVs were recorded at 0.1 V/s scan rate unless otherwise noted.

Homogeneous Electrochemical Studies. Cyclic voltammetry was carried out using a conventional three-electrode cell with a GC working electrode (surface area = 0.07 cm²), nonaqueous Ag/0.01 M AgNO₃ in a MeCN reference electrode, and Pt-wire counter electrode. The GC electrode was prepared by polishing on a cloth polishing pad using 5-micron aluminum oxide polishing slurry, followed by a thorough deionized water rinsing and gentle drying with a heat gun.²⁹ CVs were recorded by dissolving **1•PF₆** to 1.5 mM concentration with 0.1 M ^tBu₄NPF₆ (TBAPF₆) in dry MeCN, unless otherwise noted. Ferrocene was used as an external standard, and all potentials were reported with respect to the ferrocenium–ferrocene couple (Fc⁺⁰).³⁰

Heterogeneous Electrochemical Studies. Cyclic voltammetry was carried out using a conventional three-electrode cell with an EPG working electrode (surface area = 0.09 cm²), aqueous AgCl/Ag reference electrode, and a carbon rod or GC counter electrode. The EPG electrodes were polished and prepared following the procedures reported in the literature.^{22,23} A 20 μL aliquot of 1.5 mM **1** in MeCN was drop-cast

onto the EPG working electrode, dried to evaporate the solvent residues, and rinsed thoroughly with deionized water to remove any loosely bound molecules on the electrode surface. All heterogeneous electrochemical experiments were studied in 1 M H₂SO₄ aqueous solution at pH 0 after saturating in either the N₂ or O₂ atmosphere. All potentials for heterogeneous electrochemical experiments were reported with respect to the NHE.

RESULTS AND DISCUSSION

Homogeneous Electrochemical ORR Studies. *Cyclic Voltammetry Studies under N₂.* The initial electrochemical studies were performed under N₂ by dissolving [(^tBuN4)-Pd^{III}MeCl]PF₆, **1**•PF₆, in 0.1 M TBAPF₆/MeCN. CVs recorded for **1** showed a reversible wave centered at 0.58 V vs Fc⁺⁰ for the Pd^{III/IV} redox couple and an irreversible redox wave at -0.45 V vs Fc⁺⁰ (Figure 2), assigned to the reduction

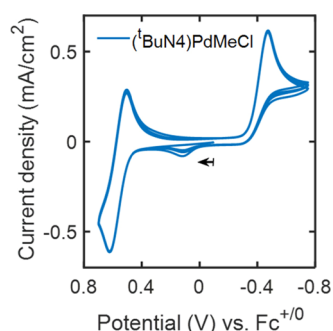


Figure 2. CVs recorded for **1** in N₂-saturated 0.1 M TBAPF₆/MeCN upon four repeating CV sweeps at the scan rate of 0.1 V/s. The black arrow shown in the figure indicates the scan direction.

of Pd^{III} to Pd^{II} based on our previous reports.²⁵ In addition, a small anodic wave at 0.14 V vs Fc⁺⁰ appeared upon repeating the CV sweeps, indicating the oxidation of Pd^{II} species formed during the reductive scans.²⁵ The irreversible nature of the Pd^{III/II} couple is likely due to the different conformers present in solution for the Pd^{II} species formed upon 1e⁻ reduction of **1**⁺ and their different redox potentials for the Pd^{II/III} oxidation, as reported previously.³¹ However, successive cyclic voltammetry cycles recorded for **1** in MeCN under N₂ showed stable peak currents for these redox features (Figure 2).

CVs were also collected for **1** in N₂-saturated MeCN at different scan rates ($\nu = 0.1$ –1 V/s, Figure 3a), and a linearity in the cathodic peak currents (i_{pc}) for the Pd^{III/IV} redox couple was observed with the square root of the scan rate ($\sqrt{\nu}$) (Figure 3b) that signifies free diffusive homogeneous processes with no significant adsorption or deposition of molecules onto the electrode surface during the cyclic voltammetry cycles.²⁹ This uncommon stability of a Pd complex under reducing conditions and the lack of any Pd metal deposition onto the cathode is unique and likely due to the hard donor atoms of the ^tBuN4 ligand and the presence of an organic methyl ligand that severely destabilizes the low oxidation states of the Pd center.

The electrochemical stability of **1** under acidic conditions was then tested by recording CVs in the presence of AcOH at different concentrations from 0.1 M and 1 M in N₂-saturated MeCN. Under these electrochemical conditions, the CVs did not show any changes of the peak potentials or degradation in peak currents, as compared to those observed in the absence of

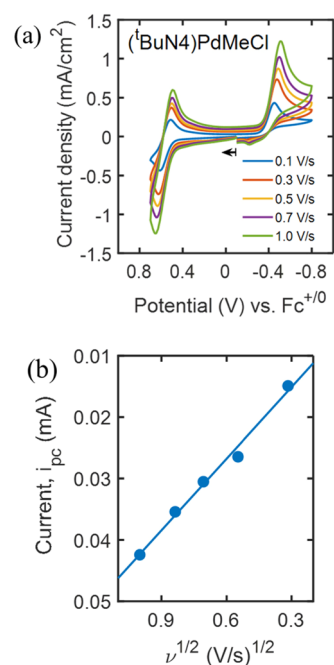


Figure 3. (a) CVs recorded for **1** in N₂-saturated MeCN at different scan rates (0.1–1 V/s). (b) Linear fit for cathodic peak currents (i_{pc}) obtained at the Pd^{III/IV} redox couple at different scan rates with the square root of the scan rate ($\nu^{1/2}$). The R^2 value for the linear fit is 0.99.

the acid (Figure 4a). Additionally, the stability of **1** was also investigated by adding 1 M of trifluoroacetic acid (TFA) or MeOH in MeCN, and no prominent changes in the CV sweeps were observed (Figures S6 and S7). Furthermore, the UV–vis absorption spectra of **1** in MeCN in the presence of different amounts of AcOH did not show any significant changes (Figure 4b). Together, these results suggest that **1** is

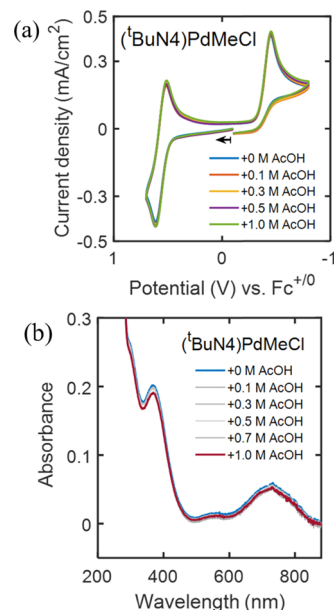


Figure 4. (a) CVs recorded for **1** in N₂-saturated 0.1 M TBAPF₆ MeCN in the absence and presence of different amounts of AcOH (0.1–1.0 M). (b) Absorption spectra for **1** in MeCN in the absence and presence of AcOH up to 1 M.

impressively stable in the presence of moderate to weak acids in MeCN, and the chelating amine arms of the ^tBuN4 ligand in **1** do not easily get protonated.²⁵

Homogeneous Electrochemical ORR in the Presence of AcOH. The CVs of **1** in O₂-saturated MeCN showed a slight increase in current densities at the peak potential of the Pd^{III/II} reductive wave, indicating a small degree of O₂ reduction in dry MeCN (Figure 5a). An additional current enhancement

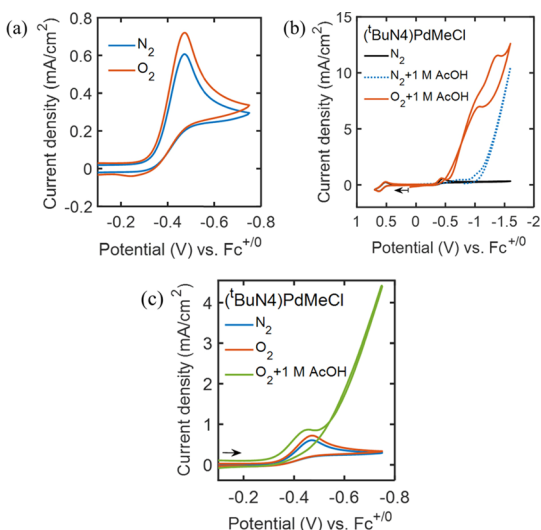


Figure 5. (a) Comparative CVs recorded for **1** in N₂- (blue) and O₂-saturated (orange) 0.1 M TBAPF₆/MeCN. (b) Same as (a) but in the presence of 1 M AcOH within the electrochemical window between 0.8 V and −1.6 V vs Fc⁺⁰. (c) Same as (a) but after the addition of 1 M AcOH in O₂-saturated MeCN. All CVs were recorded at a 0.1 V/s scan rate.

beyond −1 V vs Fc⁺⁰ was also observed, and that overlapped with the background activity of the bare GC electrode under identical electrochemical conditions (Figures S1 and S9). However, the addition of 1 M AcOH into the O₂-saturated MeCN solution of **1** moved the peak potential of the Pd^{III/II} couple toward more positive potentials, and catalytic currents near the Pd^{III/II} redox wave were observed (Figure 5c). A catalytic peak current density of 12 mA/cm² was measured at a potential of −1.39 V vs Fc⁺⁰ for the O₂-saturated MeCN solution of **1** in the presence of 1 M AcOH (Figure 5b, orange line), and this current density is comparatively higher and occurs at a less negative potential than those observed for the GC electrode in the absence of **1** (Figure S2). A control experiment carried out for **1** in N₂-sparged MeCN in the presence of 1 M AcOH revealed that the onset potential of the background proton reduction happens at a ~400 mV more negative potential compared to the CV obtained for the same solution in the presence of O₂ (Figure 5b, blue dotted line).

Interestingly, when the CV sweep was reversed after completing a reductive forward scan up to the potential of −1.6 V vs Fc⁺⁰, the return wave showed a hysteretic crossing of the forward wave in O₂-sparged MeCN in the presence of 1 M AcOH (Figure 6a). Such hysteresis behavior was more prominent at low scan rates (≤0.1 V/s), but disappeared at high scan rates (≥2 V/s, Figure 6b). It is noteworthy to mention that a similar hysteretic electrochemical crossing has also been observed during the formation of a binuclear Pd^{III} species during the methane oxidation process.³² Besides, CVs recorded for **1** using 1 M AcOH showed that the catalytic

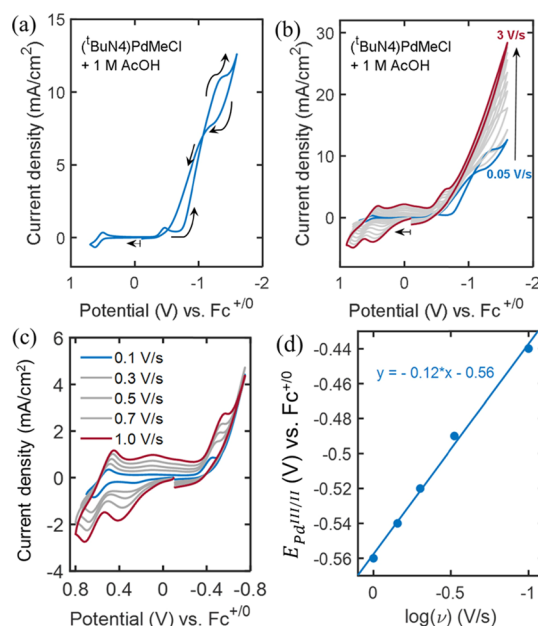


Figure 6. CVs recorded for **1** in O₂-saturated MeCN + 1 M AcOH at (a) scan rate of 0.05 V/s, (b) different scan rates (0.05–3 V/s), (c) different scan rates (0.1–1 V/s) but within the electrochemical window between 0.8 and −0.8 V vs Fc⁺⁰. (d) Linear fit obtained for cathodic peak potentials at the Pd^{III/II} redox couple at different scan rates from (c) with the logarithm of the scan rate. The R² value for the linear fit is 0.99.

redox waves moved toward more positive potentials upon repeating cyclic voltammetry cycles in the presence of O₂ (Figure S12). We hypothesize that these changes are due to the formation of thermodynamically favorable intermediates during ORR in the first CV sweep that could re-enter the next catalytic cycle of ORR events in the consecutive CV sweeps. Further discussion of the possible ORR mechanism for **1** is included below.

Additionally, new redox features around 0.4 V vs Fc⁺⁰ under the conditions mentioned above were observed, and they became more quasi-reversible as the scan rate was increased, as evidenced by the increase in the ratio of the cathodic and anodic peak current densities from 0 to 0.54, while increasing the scan rates from 0.1 to 1 V/s (Figure 6b,c). The appearance of these new redox waves near the Pd^{III/IV} redox couple could be indicative of the formation of another Pd^{III} species in solution. Such new redox features were also consistent with a similar set of CVs obtained within the electrochemical window between 0.8 and −0.8 V vs Fc⁺⁰ (Figure 6c). However, the potentials obtained at the Pd^{III/II} reductive waves at the different scan rates exhibited a linear correlation versus the logarithm of the scan rate with a slope of 120 mV/decade (Figure 6d), suggesting a proton-coupled electron transfer (PCET) process.^{19,33} Further ORR reactivity studies were performed for **1** using three different Brønsted acids, TFA (pK_a = 12.65),³⁴ AcOH (pK_a = 23.51),³⁴ and MeOH (pK_a = 37.44)³⁵ at 1 M in MeCN, and they revealed that the onset potentials of the catalytic waves maintained a correlation of 51 mV per pK_a unit of the acid used, also suggesting a Nernstian behavior corresponding to a concerted PCET process (Figure 7a,b).³⁶

RRDE Voltammetry for Homogeneous ORR. In order to benchmark the selectivity of the homogeneous ORR, we

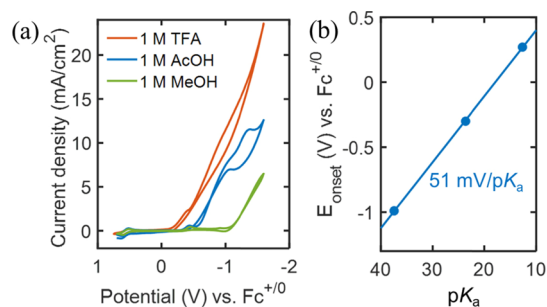


Figure 7. (a) CVs collected for **1** in O_2 -saturated MeCN in the presence of 1 M concentration of TFA (orange), AcOH (blue), and MeOH (green). (b) Onset potentials, E_{onset} (V), obtained from (a) plotted versus the pK_a values of the corresponding acid in MeCN. The R^2 value for the linear fit is 0.99.

performed RRDE experiments in O_2 -saturated MeCN in the presence of 1 M AcOH by following the methods as described by Nocera and co-workers.¹⁹ For these measurements, we used a low concentration of **1** (0.5 mM) to maintain an overall pseudo-first order reaction with respect to the dissolved O_2 concentration (~ 8.1 mM in MeCN).¹⁹ However, under such electrochemical conditions, **1** exhibited quasi-limiting disk currents at the potentials between -1.2 and -1.6 V vs $Fc^{+/0}$

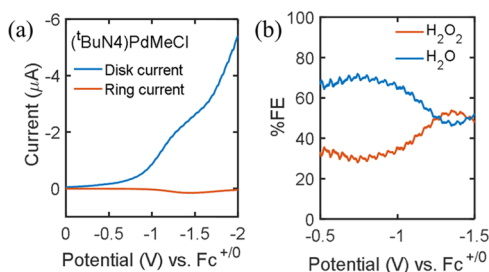


Figure 8. (a) RRDE data for **1** (0.5 mM) in O_2 -saturated 0.1 M TBAPF₆ MeCN + 1 M AcOH at the rotation rate of 150 rpm. Scan rate = 0.02 V/s. The potential at the Pt ring was held at 1 V vs reference electrode. (b) Faradaic efficiencies in percentage (%FE) for H_2O_2 and H_2O obtained from the data, as shown in (a) by using eq 1.

(Figure 8a). The Faradaic efficiency (FE) for H_2O was then estimated using the following equation, eq 1:^{19,23}

$$100 - \%H_2O_2 = 100 - \left(\frac{2 \times I_r/N}{I_d + I_r/N} \times 100 \right) \quad (1)$$

where I_d is the disk current, I_r is the ring current, and N is the collection efficiency ($= 0.18$). The maximum FE for H_2O using **1** was thus obtained as $\sim 70\%$ within the applied potentials nearer to the onset potentials, between -0.5 and -1 V vs $Fc^{+/0}$ (Figure 8b). However, the FE for H_2O was further degraded down to $\sim 50\%$ ($50\% H_2O_2$) at potentials between -1 and -1.4 V vs $Fc^{+/0}$, while the ORR activity beyond -1.5 V vs $Fc^{+/0}$ includes the background ORR contribution from the bare GC disk electrode.

FOWA and Reaction Orders for ORR Catalysis. FOWA was carried out to gain kinetic insights of the ORR process for **1**. In O_2 -saturated MeCN, **1** showed quasi-plateau current densities at different concentrations of AcOH between 0.3 M and 1.0 M (Figure S13). These CVs were then fitted using the FOWA equation (Figure 9a and Figures S16–S19), and the slopes

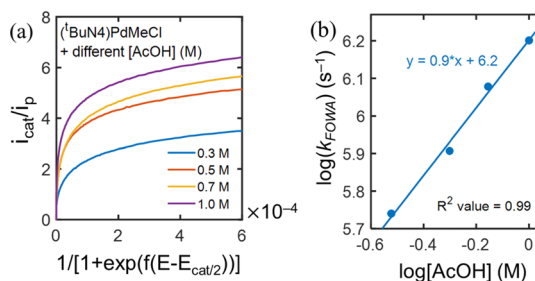
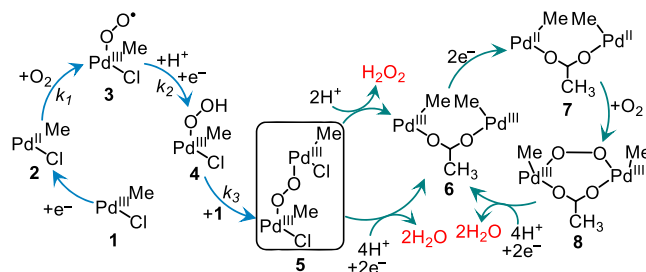


Figure 9. (a) Fitting of the FOWA equation for the CVs of **1** in O_2 -saturated MeCN in the presence of different concentrations of AcOH, 0.3 M (blue), 0.5 M (orange), 0.7 M (yellow), and 1.0 M (purple).³⁵ (b) Plot for the logarithm of k_{FOWA} as estimated from the FOWA versus the logarithm of AcOH concentration and fitted linearly. The slope of the linear fit, 0.9, indicates the first-order rate constant with respect to the acid concentration.

obtained from the FOWA provided the pseudo-first order reaction rate constants (k_{FOWA}) that can be considered as the maximum turnover frequency at a given acid concentration (Table S1).³⁵ The logarithms of these k_{FOWA} values were then plotted versus the logarithm of AcOH concentration and fitted linearly (Figure 9b), and the slope obtained from the linear fit suggests a first-order reaction with respect to the acid concentration when the concentrations of catalyst **1** (1.5 mM) and O_2 (8.1 mM in MeCN) were held constant. Such first-order reaction indicates that the first protonation step at the Pd^{III}-superoxide complex (**3**) involves one equiv. of AcOH that drives the reaction to form the Pd^{III}-hydroperoxo intermediate **4** (Scheme 1), as discussed below.

Scheme 1. Proposed Mechanism for ORR Using **1** in O_2 -Saturated MeCN in the Presence of 1 M AcOH. The Chelating ^tBuN₄ Ligand Is Omitted for Clarity^a



^aAn alternate ORR catalytic mechanism could involve binuclear Pd complexes, in which the two Pd centers are not bridged by an acetate group, similar to intermediate **5**

Similarly, keeping the concentration of AcOH (1.0 M) constant in O_2 -saturated MeCN, CVs recorded at low concentrations of **1** (0.12, 0.17, 0.22, and 0.32 mM) showed that the onset potential moved toward more positive potential with a slight increase in the quasi-limiting currents as the catalyst concentration was increased (Figure S14). The apparent reaction rate constants (k_{ap}) was estimated under these conditions using a modified FOWA equation (eq S14 and Table S2),^{35,37} and variation of k_{ap} was then fitted linearly with the varying concentration of catalysts, and the slope of the linear fit was determined to be ~ 1.7 , thus suggesting an ORR reaction that is second-order with respect to the catalyst (Figure 10). A similar second-order ORR reaction was observed for an iron-porphyrin catalyst where a peroxo-

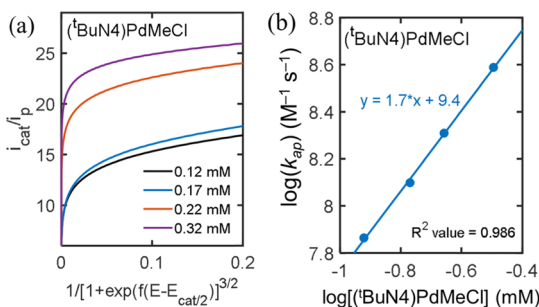


Figure 10. (a) Fitting of FOWA equation for the CVs of **1** at different concentrations, 0.12 mM (black), 0.17 mM (blue), 0.22 mM (orange), and 0.32 mM (purple) in O_2 -saturated MeCN + 1 M AcOH.³⁵ (b) Plot for logarithm of k_{ap} , as estimated from the FOWA versus the logarithm of catalyst concentration and fitted linearly. The slope of the linear fit, 1.7, indicates a primarily second-order ORR process with respect to the catalyst.

bridged Fe^{III} porphyrin dimer becomes a key intermediate toward H_2O_2 formation.³⁸ Moreover, the second-order dependence of the reaction on the catalyst concentration also supports our proposal for the formation of a binuclear Pd intermediate, most likely a binuclear Pd^{III} -peroxo- Pd^{III} species (**5**).

Investigation of the ORR Mechanism in MeCN in the Presence of AcOH. Based on our electrochemical data and literature reports, we propose an overall electrochemical mechanism for ORR for the organometallic Pd^{III} complex **1** as outlined in Scheme 1. The catalytic cycle begins upon the $1e^-$ reduction of **1** to form $(^t\text{BuN4})\text{Pd}^{\text{II}}\text{MeCl}$ (**2**), which can react with O_2 , as the slight increase in the current densities was observed at the redox couple of $\text{Pd}^{\text{III/II}}$ in dry MeCN (Figure 5a). The adduct formed after the O_2 binding at the Pd^{II} center can be described as a Pd^{III} -superoxide complex (**3**),²⁶ which then can undergo a faster PCET process in the presence of an acid to yield complex **4** in the precatalytic ORR step. The appearance of a new quasi-reversible redox wave prior to the reversible $\text{Pd}^{\text{III/IV}}$ redox couple in the presence of O_2 and acid suggests the formation of a new high valent Pd species (Figures 6b,c) that can be tentatively assigned to a binuclear Pd^{III} -peroxo- Pd^{III} complex (**5**) as a result of the reaction between complexes **4** and excess **1** in the bulk electrolyte. Thus, the appearance of two redox couples within the electrochemical window between 0 and 0.8 V vs $\text{Fc}^{+/0}$ in the presence of O_2 and AcOH could be ascribed as sequential $1e^-$ redox events for the two Pd^{III} centers of complex **5**, in line with what was reported previously for binuclear Pd^{III} complexes that exhibit similar CVs.³⁹

The proposed binuclear Pd^{III} -peroxo- Pd^{III} intermediate **5** is sensitive to the acid concentration and generates H_2O_2 with a maximum FE of 30%, as observed in the RRDE experiments at potentials between the onset potential and -1.0 V vs $\text{Fc}^{+/0}$. However, within these applied potentials, H_2O was obtained as the major product at the beginning of the ORR process, and hence, we propose that complex **5** also can be reduced by 4H^+ and $2e^-$ to form two molecules of H_2O and complex **6**. We propose that complex **6** is most likely a binuclear Pd^{III} complex bridged with an acetate residue after replacing ligated Cl^- ions in the presence of high AcOH concentration in O_2 -saturated MeCN, although a mononuclear $\text{Pd}^{\text{III}}\text{Me}(\text{OAc})$ complex cannot be excluded. Further reductive scanning in the forward CV sweep during the ORR process could lead to a $2e^-$

reduction of **6** to yield the Pd^{II} complex **7**, which should also be able to interact with O_2 and thus start a new catalytic ORR cycle. The reaction of **7** with O_2 could generate a binuclear Pd^{III} -peroxo- Pd^{III} complex **8**, which could undergo a $4\text{H}^+/2e^-$ reduction event to generate water and complex **6**, thus closing the catalytic ORR cycle. The participation of complex **6** into the next ORR cycle is expected to shift the catalytic wave toward more positive potential (or less overpotential) upon repeating cyclic voltammetry cycles (Figure S12). In addition, an alternate ORR catalytic mechanism could be envisioned that involves binuclear Pd species similar to **6**, **7**, and **8**, yet in which the two Pd centers are not bridged by an acetate group, analogous to species **5**.

Heterogeneous Electrochemical ORR Studies. *Cyclic Voltammetry Studies under N_2 .* To investigate the heterogeneous electrochemical activity of our **1** toward ORR, we immobilized our molecular catalyst by drop-casting onto the EPG electrodes using the methodology as described in the literature^{22,23} (see Experimental Details Section). All the electrochemical experiments for heterogeneous ORR were carried out in 1 M H_2SO_4 aqueous solution at pH 0 after saturating with either N_2 or O_2 . CVs collected for **1** adsorbed onto the EPG surface in N_2 -saturated aqueous electrolyte showed a quasi-reversible redox wave centered at 0.63 V vs NHE with the peak separation of 89 mV, which could be attributed to the $\text{Pd}^{\text{III/II}}$ redox couple (Figure 11a). The

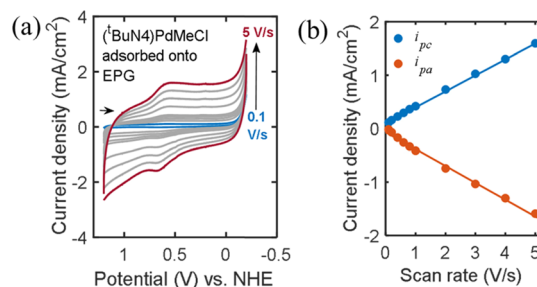


Figure 11. (a) CVs recorded for **1** adsorbed onto EPG in N_2 -saturated 1 M H_2SO_4 aqueous solution at different scan rates (0.1–5 V/s). (b) Peak currents obtained for $\text{Pd}^{\text{III/II}}$ redox couple were plotted versus the scan rate (V/s). The R^2 values for the linear fit of cathodic (i_{pc}) and anodic peak current densities (i_{pa}) are 0.998 and 0.994, respectively.

reversibility at the $\text{Pd}^{\text{III/II}}$ redox wave became more prominent as the scan rate was increased up to 5 V/s, and peak current densities obtained for $\text{Pd}^{\text{III/II}}$ redox couples at different scan rates showed a linear correlation with the scan rate (Figure 11b), indicating the efficient immobilization of the catalyst onto the surface.^{23,29} Peak current densities for this reversible wave were stable upon repeating CV sweeps (Figure 12, blue), and the electroactive species adsorbed onto the surface of the electrode, $\Gamma = (Q_{\text{CV}}/nFA)$, was estimated as 1.65×10^{-10} mol/ cm^2 by considering Q_{CV} (1.44 μC) as the charge passed at the reductive $\text{Pd}^{\text{III/II}}$ wave in the N_2 -saturated aqueous electrolyte, where n is the number of electrons (equal to 1 for the $\text{Pd}^{\text{III/II}}$ couple), F is the Faraday constant, and A is the surface of the EPG electrode (0.09 cm^2).⁴⁰

Cyclic Voltammetry Studies under O_2 . The CVs collected for **1** immobilized onto the EPG electrode in O_2 -saturated acidic medium showed a ca. fivefold current enhancement at 0.03 V vs NHE when compared to CVs recorded under N_2 (Figure 12). The peak currents observed for surface-deposited

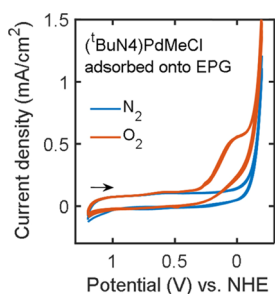


Figure 12. Comparative CVs recorded for **1** immobilized onto the EPG surface in (blue) N_2 - and (orange) O_2 -saturated 1 M H_2SO_4 aqueous solution (pH 0) upon four repeating CV sweeps. All CVs were recorded at a 0.1 V/s scan rate. The arrow shown in the figure indicates the direction of these cyclic voltammetry scans.

1 showed no current degradation in the presence of O_2 when subsequent cyclic voltammetry cycles were collected under identical electrochemical conditions (Figure 12). It is worth noting that the peak potential observed for **1** adsorbed onto the EPG electrode was 270 mV more positive than that of the bare EPG electrode in O_2 -sparged 1 M H_2SO_4 aqueous solution (Figure S26).

RRDE Voltammetry for Heterogeneous ORR. The selectivity of **1** toward heterogeneous electrochemical O_2 reduction was also studied by carrying out RRDE experiments after drop-casting the catalyst onto a GC disk using 0.1% weight equivalent of Nafion as an adhesive. An unmodified Pt-ring electrode was used in the RRDE experiments, and the potential of the Pt-ring was kept fixed at 1.0 V vs reference electrode to make sure that all O_2 -reduced species will be oxidized back to O_2 . The RRDE results obtained for **1** immobilized on the GC disk in O_2 -saturated 1 M H_2SO_4 solution showed quasi-limiting disk currents at potentials lower than 0.3 V vs NHE, and such currents increased with the rotation rates of the disk electrodes (Figure 13a). While the

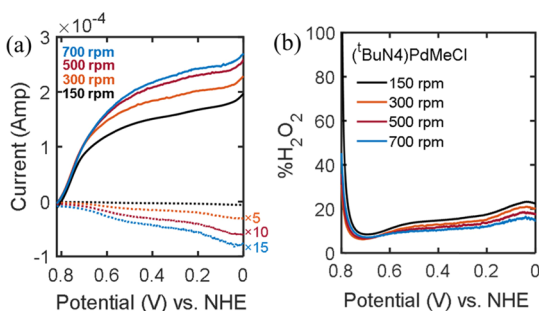


Figure 13. (a) RRDE data for **1** immobilized on a GC disk in O_2 -saturated 1 M H_2SO_4 solution at different rotation rates (ω); 150 rpm (black), 300 rpm (orange), 500 rpm (magenta), and 700 rpm (blue). The ring currents obtained at 300, 500, and 700 rpm are magnified by 5, 10, and 15 times, respectively, for clarity. Scan rate = 0.02 V/s. The potential for the Pt ring was held at 1 V vs reference electrode. (b) Faradaic efficiencies (FE) for H_2O_2 (% H_2O_2) were calculated from (a) using eq 1. % H_2O = 100 - % H_2O_2 .

onset potentials for these disk currents did not match exactly the potentials observed in the CVs recorded for **1** immobilized onto the EPG electrode in the O_2 -saturated aqueous medium (Figure 12), we assigned these differences to the different carbon surfaces used in the cyclic voltammetry and RRDE experiments, that is, the EPG electrode vs the GC electrode

with nafion used as adhesive, respectively, which could affect the degree of immobilization of **1** onto the electrode surface and hence the onset potentials. However, **1** showed comparatively low ring currents in the O_2 -saturated aqueous electrolyte under the same electrochemical conditions, suggesting higher selectivity for O_2 reduction toward H_2O formation. The Faradaic efficiency (FE) for H_2O was then calculated at different rotation rates using eq 1. When catalyst **1** was immobilized onto the GC disk electrode, an 80% FE for H_2O formation was observed at the rotation rate of 150 rpm and applied potentials lower than 0.3 V during the ORR electrocatalysis in acidic aqueous electrolyte, and the percentage of H_2O formation increased up to ~90% when the rotation of the RRDE electrode was increased up to 700 rpm (Figure 13b). Although even under optimal conditions for electrochemical ORR catalyzed by the Pd complex **1**, a small amount of H_2O_2 is still formed, which is not desirable when designing practical energy devices; the finding that a surprisingly stable high-valent organometallic Pd^{III} complex can serve as a heterogeneous catalyst for ORR under a very acidic (pH 0) aqueous environment medium, without any notable catalyst decomposition while reducing O_2 in water, is deemed to be quite unique. Detailed studies aimed at understanding the identity of complex **1** upon immobilization onto the electrode surface will be the focus of our future research efforts.

K–L Plots and ORR Kinetics. To calculate the number of electrons involved in heterogeneous ORR using our catalyst, the K–L plots, i_{lim}^{-1} versus $\omega^{-1/2}$, were constructed, where i_{lim} is the limiting disk currents observed for our catalyst-immobilized disk electrode at a given angular rotation rate (ω , Figure 14). For a better comparison, we have also included the

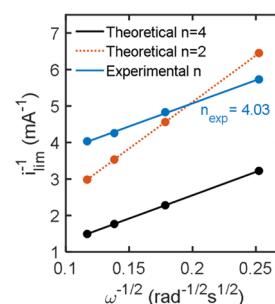
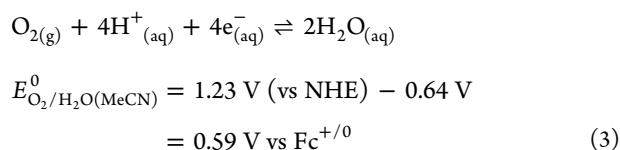
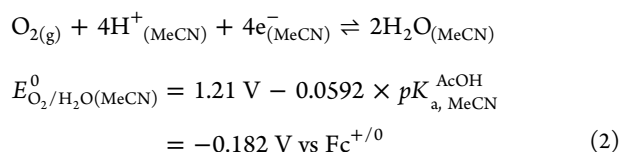


Figure 14. Koutecky–Levich (K–L) plots for **1** adsorbed onto a rotating carbon disk electrode considering the limiting currents observed at 0.1 V (blue), and the theoretical K–L plots for $2e^-$ (orange) and $4e^-$ (black) processes are shown for comparison. n_{exp} is the number of electrons involved in the ORR process estimated from the slope of the K–L plot for **1**. The R^2 values for the linear fits are 0.998 (experimental n , blue), 1.00 (theoretical $n = 2$, orange), and 1.00 (theoretical $n = 4$, black).

theoretical K–L plots corresponding to $2e^-$ and $4e^-$ events of the ORR process. The linear fit of the experimental K–L plot for **1** that adsorbed EPG at the applied potential of 0.1 V vs NHE is parallel to the theoretical K–L plot of the number of electrons, $n = 4$, suggest a $4e^-$ reduction of O_2 to H_2O . The number of electrons associated with the ORR process (n_{exp}) for the heterogeneous catalyst **1** was also extracted from the slope of the experimental K–L plots and found to be 4.03 at an applied potential of 0.1 V vs NHE (Figure 14), while a range of n_{exp} of 3.74–4.03 was found considering the quasi-limiting disk currents within the potential window between 0.2 and 0.1 V vs

NHE (Figure S28b). Moreover, the intercepts obtained from the linearly fitted experimental K–L plots were used to estimate the overall second-order reaction rate constant, k_{cat} , for our heterogeneous ORR catalyst **1**, which was found to be $1.26 \times 10^5 \text{ M}^{-1} \text{ s}^{-1}$.

Standard Potentials and Overpotential Analysis. To benchmark the thermodynamic parameters obtained for homogeneous and heterogeneous ORR using **1** in MeCN and aqueous solutions, respectively, we first calculated the standard potential ($E_{\text{O}_2/\text{H}_2\text{O}(\text{MeCN})}^0$) for the $4\text{H}^+/4\text{e}^-$ reduction of O_2 in MeCN in the presence of AcOH using eq 2.⁴¹ Considering the $\text{p}K_{\text{a}}$ of AcOH in MeCN as 23.51,³⁴ we obtained $E_{\text{O}_2/\text{H}_2\text{O}(\text{MeCN})}^0 = -0.182 \text{ V vs Fc}^{+/0}$. However, the standard potential for the same redox reaction in aqueous medium is +1.23 V vs NHE,⁴² which can be referenced as +0.59 V vs $\text{Fc}^{+/0}$, by subtracting -0.64 V according to eq 3.³⁰



Considering these standard potentials (vs $\text{Fc}^{+/0}$) for the reduction of O_2 to water in MeCN and aqueous electrolyte, we then estimated the overpotentials for the ORR catalyzed by **1** within the applied potential (E_{applied}) between the onset (E_{onset}) and the catalytic peak potential (E_{cat} , Figure 15). For the

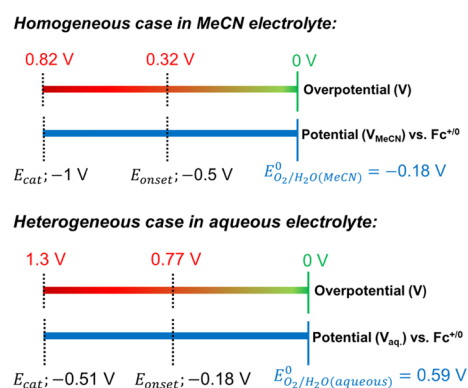


Figure 15. Calculated diagrams for **1** to estimate the overpotentials involved in homogeneous (top) and heterogeneous (bottom) ORR processes in 0.1 M TBAPF₆/MeCN and 1 M H₂SO₄ aqueous solution (pH 0), respectively. The potential windows for both cases are referenced versus $\text{Fc}^{+/0}$ for a better comparison.

homogeneous case, **1** exhibited an overpotential ($E_{\text{O}_2/\text{H}_2\text{O}(\text{MeCN})}^0 - E_{\text{applied}}$) within the range of 0.32 and 0.82 V (Figure 15, top). By contrast, the estimated overpotential ($E_{\text{O}_2/\text{H}_2\text{O}(\text{aqueous})}^0 - E_{\text{applied}}$) for **1** immobilized onto the EPG electrode is comparatively much higher and in between 0.77 and 1.3 V (Figure 15, bottom). The rationale to support the less-than-optimal thermochemistry obtained for **1** in the heterogeneous case is not known at this time because the nature of the adsorbed catalyst still needs to be better characterized.

However, the observation that **1** is a better ORR electrocatalyst in solution in terms of both lower overpotential and higher turnover frequency than when immobilized on the electrode surface further supports the formation of a dinuclear intermediate species that may not form easily on the electrode surface.

CONCLUSIONS

In conclusion, herein, we report an organometallic Pd^{III} complex, [(^tBuN₄)Pd^{III}MeCl]PF₆, **1**•PF₆, as a molecular and heterogeneous ORR catalyst in organic and aqueous medium using graphite electrodes that are earth-abundant and less expensive than the typical Pt-based cathode catalysts commonly used in fuel cells. The homogeneous and heterogeneous ORR reactivity of **1**•PF₆ was studied in detail, and its reactivity was benchmarked for the selective reduction of O_2 to H_2O . This complex exhibited elevated ORR kinetics in the MeCN solution in the presence of AcOH at low overpotential (0.32 V) to the onset potential. Analysis of electrochemical data suggests the formation of a binuclear Pd^{III} intermediate in solution, likely a Pd^{III}-peroxy-Pd^{III} species, which dictates the thermochemistry of the ORR process for [(^tBuN₄)Pd^{III}MeCl]⁺ in MeCN, thus being a rare example of a bimolecular ORR process. The selectivity for H_2O production under these homogeneous ORR conditions was investigated using hydrodynamic electrochemical methods, and the FE for H_2O formation was as high as 70%. Furthermore, the immobilization of the molecular Pd^{III} ORR electrocatalyst onto graphite electrodes led to the reduction of O_2 in acidic aqueous solution with an FE greater than 80% for H_2O formation. Although the overpotential observed for the heterogeneous case is comparatively high, the performance of an organometallic Pd^{III} complex toward O_2 reduction under strong acidic conditions is impressive in terms of its catalytic stability, selectivity, and turnover frequency. This uncommon stability of the Pd complex **1**•PF₆ under reducing conditions and the lack of any Pd metal deposition is unique and likely due to the hard donor atoms of the ^tBuN₄ ligand and the presence of an organic methyl ligand that severely destabilizes the low oxidation states of the Pd center. Overall, these studies suggest that organometallic molecular Pd catalysts could be potentially used in paired electrolysis applications to couple the ORR with oxidative organometallic transformations of interest to the chemical and petroleum industry.

ASSOCIATED CONTENT

Supporting Information

The Supporting Information is available free of charge at <https://pubs.acs.org/doi/10.1021/acscatal.0c05726>.

Detailed experimental details for the homogenous and heterogeneous electrochemical studies and foot-of-the-wave analyses (PDF)

AUTHOR INFORMATION

Corresponding Author

Liviu M. Mirica – Department of Chemistry, University of Illinois at Urbana-Champaign, Urbana, Illinois 61801, United States; orcid.org/0000-0003-0584-9508; Email: mirica@illinois.edu

Author

Soumalya Sinha – Department of Chemistry, University of Illinois at Urbana-Champaign, Urbana, Illinois 61801, United States

Complete contact information is available at:
<https://pubs.acs.org/10.1021/acscatal.0c05726>

Notes

The authors declare no competing financial interest.

ACKNOWLEDGMENTS

We thank the University of Illinois for supporting the initial studies described herein. We acknowledge Prof. Andrew A. Gewirth and Prof. Joaquín Rodríguez-López and their research groups for allowing us access to their rotating-ring disk electrode setups. We also thank Prof. Jeffrey J. Warren for providing us the edge plane graphite electrodes.

REFERENCES

- (1) Behling, N. H. In *Fuel Cells*; Behling, N. H., Ed.; Elsevier, 2013, 7.
- (2) Winter, M.; Brodd, R. J. What Are Batteries, Fuel Cells, and Supercapacitors? *Chem. Rev.* **2004**, *104*, 4245.
- (3) Lewis, N. S.; Nocera, D. G. Powering the planet: Chemical challenges in solar energy utilization. *Proc. Natl. Acad. Sci. U. S. A.* **2006**, *103*, 15729.
- (4) Devivaraprasad, R.; Nalajala, N.; Bera, B.; Neergat, M. Electrocatalysis of Oxygen Reduction Reaction on Shape-Controlled Pt and Pd Nanoparticles—Importance of Surface Cleanliness and Reconstruction. *Front. Chem.* **2019**, *70*, No. 00648.
- (5) Borup, R.; Meyers, J.; Pivovar, B.; Kim, Y. S.; Mukundan, R.; Garland, N.; Myers, D.; Wilson, M.; Garzon, F.; Wood, D.; Zelenay, P.; More, K.; Stroh, K.; Zawodzinski, T.; Boncella, J.; McGrath, J. E.; Inaba, M.; Miyatake, K.; Hori, M.; Ota, K.; Ogumi, Z.; Miyata, S.; Nishikata, A.; Siroma, Z.; Uchimoto, Y.; Yasuda, K.; Kimijima, K.-i.; Iwashita, N. Scientific Aspects of Polymer Electrolyte Fuel Cell Durability and Degradation. *Chem. Rev.* **2007**, *107*, 3904.
- (6) Dey, S.; Mondal, B.; Chatterjee, S.; Rana, A.; Amanullah, S.; Dey, A. Molecular electrocatalysts for the oxygen reduction reaction. *Nat. Rev. Chem.* **2017**, *1*, 0098.
- (7) Mittermeier, T.; Weiß, A.; Gasteiger, H. A.; Hasché, F. Monometallic Palladium for Oxygen Reduction in PEM Fuel Cells: Particle-Size Effect, Reaction Mechanism, and Voltage Cycling Stability. *J. Electrochem. Soc.* **2017**, *164*, F1081.
- (8) Siebel, A.; Gorlin, Y.; Durst, J.; Proux, O.; Hasché, F.; Tromp, M.; Gasteiger, H. A. Identification of Catalyst Structure during the Hydrogen Oxidation Reaction in an Operating PEM Fuel Cell. *ACS Catal.* **2016**, *6*, 7326.
- (9) Durst, J.; Simon, C.; Hasché, F.; Gasteiger, H. A. Hydrogen Oxidation and Evolution Reaction Kinetics on Carbon Supported Pt, Ir, Rh, and Pd Electrocatalysts in Acidic Media. *J. Electrochem. Soc.* **1970**, *8*, 259.
- (10) Stonehart, P. Electrocatalyst advances for hydrogen oxidation in phosphoric acid fuel cells. *Int. J. Hydrogen Energy* **1984**, *9*, 921.
- (11) Nørskov, J. K.; Rossmeisl, J.; Logadottir, A.; Lindqvist, L.; Kitchin, J. R.; Bligaard, T.; Jónsson, H. Origin of the Overpotential for Oxygen Reduction at a Fuel-Cell Cathode. *J. Phys. Chem. B* **2004**, *108*, 17886.
- (12) Zhang, J.; Vukmirovic, M. B.; Xu, Y.; Mavrikakis, M.; Adzic, R. R. Controlling the Catalytic Activity of Platinum-Monolayer Electrocatalysts for Oxygen Reduction with Different Substrates. *Angew. Chem. Int. Ed.* **2005**, *44*, 2132.
- (13) Yang, J.; Lee, J. Y.; Zhang, Q.; Zhou, W.; Liu, Z. Carbon-Supported Pseudo-Core-Shell Pd-Pt Nanoparticles for ORR with and without Methanol. *J. Electrochem. Soc.* **2008**, *155*, B776.
- (14) Oezaslan, M.; Hasché, F.; Strasser, P. Pt-Based Core-Shell Catalyst Architectures for Oxygen Fuel Cell Electrodes. *J. Phys. Chem. Lett.* **2013**, *4*, 3273.
- (15) Cherevko, S.; Zeradjanin, A. R.; Topalov, A. A.; Kulyk, N.; Katsounaros, I.; Mayrhofer, K. J. J. Dissolution of Noble Metals during Oxygen Evolution in Acidic Media. *ChemCatChem* **2014**, *6*, 2219.
- (16) Grdeń, M.; Łukaszewski, M.; Jerkiewicz, G.; Czerwiński, A. Electrochemical behaviour of palladium electrode: Oxidation, electro-dissolution and ionic adsorption. *Electrochim. Acta* **2008**, *53*, 7583.
- (17) Pizzutilo, E.; Geiger, S.; Freakley, S. J.; Mingers, A.; Cherevko, S.; Hutchings, G. J.; Mayrhofer, K. J. J. Palladium electro-dissolution from model surfaces and nanoparticles. *Electrochim. Acta* **2017**, *229*, 467.
- (18) Pegis, M. L.; Wise, C. F.; Martin, D. J.; Mayer, J. M. Oxygen Reduction by Homogeneous Molecular Catalysts and Electrocatalysts. *Chem. Rev.* **2018**, *118*, 2340.
- (19) Passard, G.; Dogutan, D. K.; Qiu, M.; Costentin, C.; Nocera, D. G. Oxygen Reduction Reaction Promoted by Manganese Porphyrins. *ACS Catal.* **2018**, *8*, 8671.
- (20) Carver, C. T.; Matson, B. D.; Mayer, J. M. Electrocatalytic Oxygen Reduction by Iron Tetra-arylporphyrins Bearing Pendant Proton Relays. *J. Am. Chem. Soc.* **2012**, *134*, 5444.
- (21) Matson, B. D.; Carver, C. T.; Von Ruden, A.; Yang, J. Y.; Raugei, S.; Mayer, J. M. Distant protonated pyridine groups in water-soluble iron porphyrin electrocatalysts promote selective oxygen reduction to water. *Chem. Commun.* **2012**, *48*, 11100.
- (22) Sinha, S.; Aaron, M. S.; Blagojevic, J.; Warren, J. J. Electrocatalytic Dioxxygen Reduction by Carbon Electrodes Non-covalently Modified with Iron Porphyrin Complexes: Enhancements from a Single Proton Relay. *Chem. A Eur. J.* **2015**, *21*, 18072.
- (23) Sinha, S.; Ghosh, M.; Warren, J. J. Changing the Selectivity of O₂ Reduction Catalysis with One Ligand Heteroatom. *ACS Catal.* **2019**, *9*, 2685.
- (24) Zhang, R.; Warren, J. J. Controlling the Oxygen Reduction Selectivity of Asymmetric Cobalt Porphyrins by Using Local Electrostatic Interactions. *J. Am. Chem. Soc.* **2020**, *142*, 13426.
- (25) Khusnutdinova, J. R.; Rath, N. P.; Mirica, L. M. Stable Mononuclear Organometallic Pd(III) Complexes and Their C-C Bond Formation Reactivity. *J. Am. Chem. Soc.* **2010**, *132*, 7303.
- (26) Khusnutdinova, J. R.; Rath, N. P.; Mirica, L. M. The Aerobic Oxidation of a Pd(II) Dimethyl Complex Leads to Selective Ethane Elimination from a Pd(III) Intermediate. *J. Am. Chem. Soc.* **2012**, *134*, 2414.
- (27) Tang, F.; Zhang, Y.; Rath, N. P.; Mirica, L. M. Detection of Pd(III) and Pd(IV) Intermediates during the Aerobic Oxidative C-C Bond Formation from a Pd(II) Dimethyl Complex. *Organometallics* **2012**, *31*, 6690.
- (28) Schultz, J. W.; Rath, N. P.; Mirica, L. M. Improved Oxidative C-C Bond Formation Reactivity of High-Valent Pd Complexes Supported by a Pseudo-Tridentate Ligand. *Inorg. Chem.* **2020**, *59*, 11782.
- (29) Elgrishi, N.; Rountree, K. J.; McCarthy, B. D.; Rountree, E. S.; Eisenhart, T. T.; Dempsey, J. L. A Practical Beginner's Guide to Cyclic Voltammetry. *J. Chem. Educ.* **2018**, *95*, 197.
- (30) Pavlishchuk, V. V.; Addison, A. W. Conversion constants for redox potentials measured versus different reference electrodes in acetonitrile solutions at 25°C. *Inorg. Chim. Acta* **2000**, *298*, 97.
- (31) Khusnutdinova, J. R.; Rath, N. P.; Mirica, L. M. The Conformational Flexibility of the Tetradentate Ligand ^{tbu}N4 is Essential for the Stabilization of (^{tbu}N4)Pd^{III} Complexes. *Inorg. Chem.* **2014**, *53*, 13112.
- (32) O'Reilly, M. E.; Kim, R. S.; Oh, S.; Surendranath, Y. Catalytic Methane Monofunctionalization by an Electrogenerated High-Valent Pd Intermediate. *ACS Cent. Sci.* **2017**, *3*, 1174.
- (33) Bard, A. J.; Faulkner, L. R. *Electrochemical Methods: Fundamentals and Applications*; 2nd ed.; Wiley, 2008.
- (34) McCarthy, B. D.; Martin, D. J.; Rountree, E. S.; Ullman, A. C.; Dempsey, J. L. Electrochemical Reduction of Brønsted Acids by

Glassy Carbon in Acetonitrile—Implications for Electrocatalytic Hydrogen Evolution. *Inorg. Chem.* **2014**, *53*, 8350.

(35) See Supporting Information.

(36) Ngo, K. T.; McKinnon, M.; Mahanti, B.; Narayanan, R.; Grills, D. C.; Ertem, M. Z.; Rochford, J. Turning on the Protonation-First Pathway for Electrocatalytic CO₂ Reduction by Manganese Bipyridyl Tricarbonyl Complexes. *J. Am. Chem. Soc.* **2017**, *139*, 2604.

(37) Costentin, C.; Drouet, S.; Robert, M.; Saveant, J. M. Turnover numbers, turnover frequencies, and overpotential in molecular catalysis of electrochemical reactions. Cyclic voltammetry and preparative-scale electrolysis. *J. Am. Chem. Soc.* **2012**, *134*, 11235.

(38) Chin, D.-H.; La Mar, G. N.; Balch, A. L. Mechanism of autoxidation of iron(II) porphyrins. Detection of a peroxo-bridged iron(III) porphyrin dimer and the mechanism of its thermal decomposition to the oxo-bridged iron(III) porphyrin dimer. *J. Am. Chem. Soc.* **1980**, *102*, 4344.

(39) Dudkina, Y. B.; Mikhaylov, D. Y.; Gryaznova, T. V.; Tufatullin, A. I.; Kataeva, O. N.; Vivic, D. A.; Budnikova, Y. H. Electrochemical Ortho Functionalization of 2-Phenylpyridine with Perfluorocarboxylic Acids Catalyzed by Palladium in Higher Oxidation States. *Organometallics* **2013**, *32*, 4785.

(40) Maurin, A.; Robert, M. Noncovalent Immobilization of a Molecular Iron-Based Electrocatalyst on Carbon Electrodes for Selective, Efficient CO₂-to-CO Conversion in Water. *J. Am. Chem. Soc.* **2016**, *138*, 2492.

(41) Machan, C. W. Advances in the Molecular Catalysis of Dioxygen Reduction. *ACS Catal.* **2020**, *10*, 2640.

(42) Pegis, M. L.; Roberts, J. A. S.; Wasylenko, D. J.; Mader, E. A.; Appel, A. M.; Mayer, J. M. Standard Reduction Potentials for Oxygen and Carbon Dioxide Couples in Acetonitrile and N, N-Dimethylformamide. *Inorg. Chem.* **2015**, *54*, 11883.